ECOsystem Spaceborne Thermal Radiometer Experiment on Space Station (ECOSTRESS)

ECOSTRESS Level-3 DisALEXI-JPL Evapotranspiration (ECO3ETALEXI) Algorithm Theoretical Basis Document

Version 1
May 20, 2021

Kerry Cawse-Nicholson
ECOSTRESS Science Team
Jet Propulsion Laboratory
California Institute of Technology

Martha Anderson
ECOSTRESS Algorithm Development Team
ECOSTRESS Science Team
U.S. Department of Agriculture
Agricultural Research Service

National Aeronautics and Space Administration

Jet Propulsion Laboratory
California Institute of Technology
Pasadena, California

This research was carried out at the Jet Propulsion Laboratory, California Institute of Technology, under a contract with the National Aeronautics and Space Administration.

Contacts

Readers seeking additional information about this document may contact the following ECOSTRESS Science Team members:

- Kerry Cawse-Nicholson
  MS 183-501
  Jet Propulsion Laboratory
  4800 Oak Grove Dr.
  Pasadena, CA 91109
  Email: Kerry-anne.cawse-nicholson@jpl.nasa.gov
  Office: (818) 354-1594

- Martha C. Anderson
  Hydrology and Remote Sensing Laboratory
  USDA - ARS
  103000 Baltimore Ave
  Beltsville, MD 20705
  Email: martha.anderson@ars.usda.gov
  Office: (301) 504-6616

- Simon J. Hook
  MS 183-501
  Jet Propulsion Laboratory
  4800 Oak Grove Dr.
  Pasadena, CA 91109
  Email: simon.j.hook@jpl.nasa.gov
  Office: (818) 354-0974
  Fax: (818) 354-5148

List of Acronyms

ALEXI	Atmosphere–Land Exchange Inverse
ARS	Agricultural Research Service
ATBD	Algorithm Theoretical Basis Document
Cal/Val	Calibration and Validation
CDL	Cropland Data Layer
CFSR	Climate Forecast System Reanalysis
CONUS	Contiguous United States
DisALEXI-JPL	Disaggregated ALEXI algorithm
ECOSTRESS	ECOsystem Spaceborne Thermal Radiometer Experiment on Space Station
ET	Evapotranspiration
EVI-2	Earth Ventures Instruments, Second call
GET-D	GOES Evapotranspiration and Drought System
HRSL	Hydrology and Remote Sensing Laboratory
ISS	International Space Station
L-2	Level 2
L-3	Level 3
LSTE	Land-surface Temperature and Emissivity
LTAR	Long-Term Agroecosystem Research
MODIS	MODerate-resolution Imaging Spectroradiometer
NASS	National Agricultural Statistics Service
NLCD	National Land Cover Dataset
NOAA	National Oceanographic and Atmospheric Administration
PM	Penman-Monteith
RMSD	Root Mean Squared Difference
SEB	Surface Energy Balance
TIR	Thermal Infrared
TSEB	Two-Source Energy Balance
USDA	United States Department of Agriculture

Contents

1 Introduction

1.1 Purpose

Evapotranspiration (ET) is one of the primary science output variables by the ECOsystem Spaceborne Thermal Radiometer Experiment on Space Station (ECOSTRESS) mission (Fisher et al. 2014; Fisher et al., 2020). ET is a Level-3 (L-3) product constructed from a combination of the ECOSTRESS Level-2 (L-2) land surface temperature and emissivity (*LSTE*) product (*Hulley* et al. 2018) and ancillary data products. ET is determined by many environmental and biological controls, including net radiation, meteorological conditions, soil moisture availability, and vegetation characteristics (e.g., type, amount, and health). While there are many approaches for mapping ET spatially, methods based on surface energy balance (SEB) are best suited for remote sensing retrievals based on land-surface temperature (Kalma et al. 2008; Kustas and Anderson 2009). The SEB approach answers the question: Given an estimate of the radiation load on a given patch on the land surface, how much evaporative cooling is required to keep the soil and vegetation (and other) components of that patch at the radiometric temperature observed from a remote sensing platform? In this Algorithm Theoretical Basis Document (ATBD), we describe a surface energy balance approach that is utilized by the ECOSTRESS mission to retrieve ET over agricultural sites within the United States. The algorithm described here (DisALEXI-JPL) is based on spatial disaggregation of regional-scale fluxes from the Atmosphere Land Exchange Inverse (ALEXI) SEB model.

1.2 Scope and Objectives

In this ATBD, we provide:

1. Description of the ET dataset characteristics and requirements;
2. Justification for the choice of algorithm;
3. Description of the general form of the algorithm;
4. Required algorithm adaptations specific to the ECOSTRESS mission;
5. Required ancillary data products with potential sources and back-up sources;
6. Plan for evaluating the ET retrievals.

2 Dataset Description and Requirements

Attributes of DisALEXI-JPL ET data produced for the ECOSTRESS mission include:

- Expands upon the DisALEXI-USDA algorithm that currently produces 30 m ET over select sites, to instead produce 70 m ET over all of contiguous United States (CONUS);
- Upscaled to daily total ET from instantaneous retrievals using radiometric temperature data collected at the overpass time of the International Space Station (ISS);
- Latency as required by the ECOSTRESS Science Data System (SDS) processing system;

3 Algorithm Selection

The ET algorithm must satisfy basic criteria to be applicable for the ECOSTRESS mission:

- Physics based and generally applicable (does not require tuning to a particular area);
- High accuracy within targeted regions;
- High sensitivity and dependency on remote sensing measurements;
- Relative simplicity necessary for high volume processing;
- Published record of algorithm maturity, stability, and validation.

The multiscale ALEXI/DisALEXI SEB model has been evaluated using tower and aircraft flux observations in the U.S. and Europe and shows good agreement (Anderson et al. 1997; 2004b; 2005; 2007b; 2008; 2012; Norman et al. 2003; Cammalleri et al. 2012; 2013; 2014a; Semmens et al. 2015; Sun et al. 2017; Yang et al. 2017a; 2017b). Figure 1 shows results of comparisons between DisALEXI-JPL estimates with tower observations from 17 eddy covariance towers around CONUS, indicating good performance (Cawse Nicholson et al., in review).

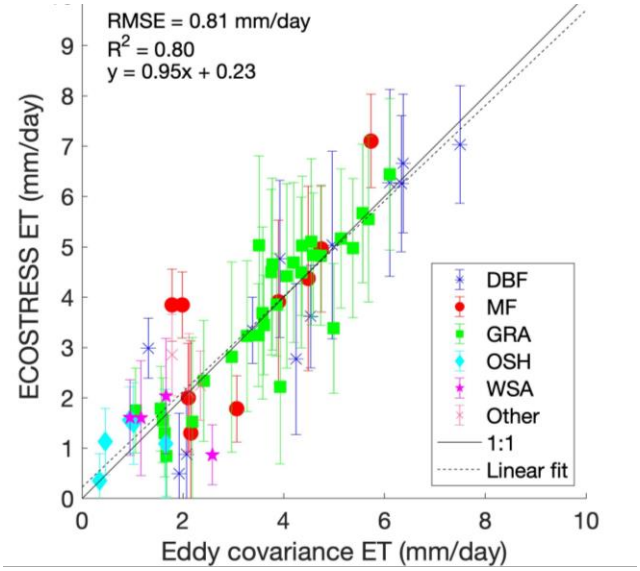

Figure 1. Comparison of tower flux measurements from 17 eddy covariance towers with model predictions from DisALEXI-JPL model.

The ALEXI/DisALEXI-JPL modeling system was selected as one of the ET algorithms for ECOSTRESS because: a) it has been identified as a robust, physically based SEB modeling system; b) it is governed primarily by remote sensing inputs of land surface temperature; c) it has demonstrated capacity for capturing signals of crop stress and related impacts on canopy temperature and transpiration fluxes; and d) it is widely used by the agricultural community.

The inherent construct of ALEXI/DisALEXI-JPL as a multiscale modeling tool provides a regional contextual basis for high-resolution ECOSTRESS ET retrievals, linking field-scale variability in water use and moisture variability across agricultural landscapes to the broader water balance and hydrological status at the continental scale (Fig. 2; Anderson et al., 2011).

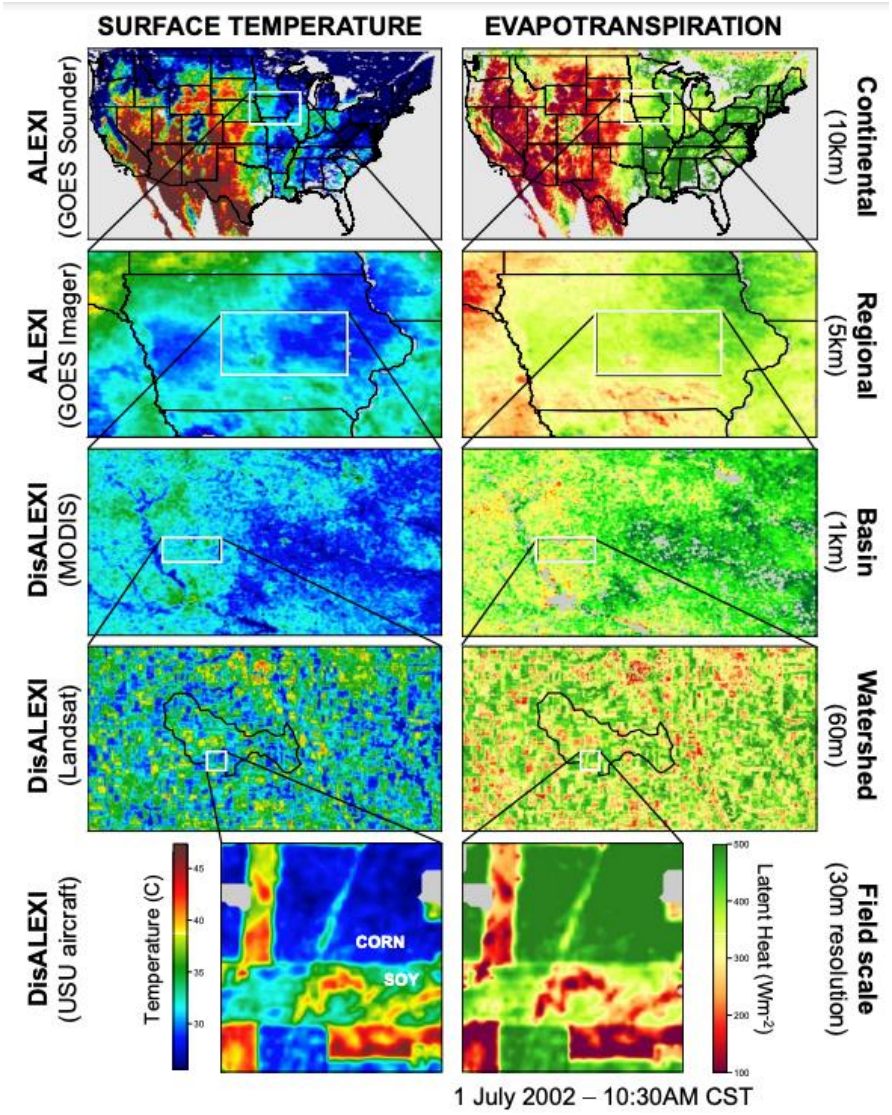

Figure 2. Multi-scale SEB ET evaluations (ALEXI/DisALEXI) using TIR data from satellites with varying spatial and temporal characteristics (Anderson et al., 2011).

4 Evapotranspiration Retrieval

The energy balance model employed here is a multi-scale system designed to generated self-consistent flux assessments from field to regional/continental scales (Anderson et al. 2003). The regional Atmosphere-Land Exchange Inverse (ALEXI) model relates time-differential LST observations from geostationary satellites to the time-integrated energy balance within the surface-atmospheric boundary layer system. ALEXI has minimal reliance on absolute (instantaneous) air or surface temperature input data, and therefore provides a relatively robust flux determination at the coarse geostationary pixel scale. For finer scale ET applications, ALEXI flux fields can be spatially disaggregated using higher resolution LST information from polar orbiting systems (e.g., Landsat or MODIS), platforms such as the ISS (e.g., ECOSTRESS), or from aircraft using an algorithm referred to as DisALEXI. Both ALEXI and DisALEXI use the Two-Source Energy Balance (TSEB) land-surface representation to partition surface fluxes between the canopy and the soil. The ALEXI/DisALEXI/TSEB system is depicted schematically in Fig.3 and described further below.

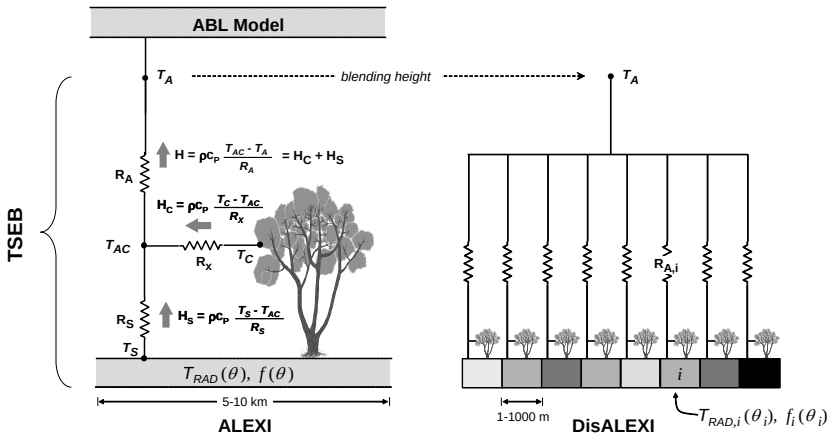

Figure 3. Schematic diagram representing the coupled ALEXI (a) and DisALEXI-JPL (b) modeling scheme, highlighting fluxes of sensible heat (*H*) from the soil and canopy (subscripts '*C*' and '*S*') along gradients in temperature (*T*), and regulated by transport resistances R_A (aerodynamic), R_X (bulk leaf boundary layer) and R_S (soil surface boundary layer). DisALEXI-JPL uses the air temperature predicted by ALEXI near the blending height (T_A) to disaggregate 5-km ALEXI fluxes, given vegetation cover ($f(\theta)$) and directional surface radiometric temperature ($T_{RAD}(\theta)$) information derived from high-resolution remote-sensing imagery at look angle θ.

4.1 Two Source Energy Balance (TSEB) land-surface model

Surface energy balance models estimate ET by partitioning the energy available at the land surface ($RN - G$, where RN is net radiation and G is the soil heat flux, both in Wm^{-2}) into turbulent fluxes of sensible and latent heating (H and λE, respectively, in Wm^{-2}):

$$RN - G = H + \lambda E \qquad \text{(Eq. 1)}$$

where λ is the latent heat of vaporization required to evaporate 1 mm of water (J kg^{-1}) and E is ET (kg s^{-1} m^{-2} or mm s^{-1}). Surface temperature is a valuable metric for constraining λE because varying soil moisture conditions yield a distinctive thermal signature. Moisture deficiencies in the rootzone lead to vegetation stress and elevated canopy temperatures, while depleted water in the soil surface layer causes the soil component of the scene to heat rapidly. Typically, LST is used to constrain the sensible heat flux estimate, while latent heat is computed as a residual in Eq. 1.

The Two-Source Energy Balance (TSEB) model of Norman et al. (1995b; Kustas and Norman 1999, 2000) further breaks down total λE into estimates of soil evaporation (λE_S) and canopy transpiration (λE_C). The TSEB partitions the composite surface radiometric temperature, T_{RAD}, obtained from thermal measurements into characteristic soil and canopy temperatures, T_S and T_C, based on the local vegetation cover fraction apparent at the sensor view angle, $f(\theta)$:

$$T_{RAD}(\theta) \approx (f(\theta)T_C{}^4 + [1 - f(\theta)]T_S{}^4)^{1/4} \qquad \text{(Eq. 2)}$$

(Fig. 3). For a canopy with a spherical leaf angle distribution and leaf area index (LAI), $f(\theta)$ can be approximated as

$$f(\theta) = 1 - \exp\left(\frac{-0.5\,\Omega(\theta)\,LAI}{\cos\theta}\right) \qquad \text{(Eq. 3)}$$

where $\Omega(\theta)$ is a view angle dependent clumping factor, here assigned by vegetation class (Anderson et al. 2005). With information about T_{RAD}, LAI, and radiative forcing, the TSEB evaluates the soil (subscript "s") and the canopy (subscript "c") energy budgets separately, computing system and component fluxes of net radiation ($RN=RN_C+RN_S$), sensible and latent heat ($H=H_C+H_S$ and $\lambda E=\lambda E_C+\lambda E_S$), and soil heat conduction (G). Because angular effects are incorporated into the decomposition of T_{RAD}, the TSEB can accommodate thermal data acquired at off-nadir viewing angles and can therefore be applied to both polar orbiting and geostationary satellite images.

In the TSEB model, Eqs. 2 and 3 are solved simultaneously with a set of equations describing the surface energy budget for the soil, canopy, and composite land-surface system:

System, soil, and canopy energy budgets:

$$RN = H + \lambda E + G \qquad (Eq.4)$$
$$RN_S = H_S + \lambda E_S + G \qquad (Eq.5)$$
$$RN_C = H_C + \lambda E_C \qquad (Eq.6)$$

Net radiation:

$$RN = RN_S + RN_C \quad (Eq.7)$$

$$RN = (L_d - L_u) + (S_d - S_u)$$
$$= L_d - (1-\tau_C)L_C - \tau_C L_S + (1-A)S_d \quad (Eq.8)$$

$$RN_S = (L_{d,s} - L_{u,s}) + (S_{d,s} - S_{u,s})$$
$$= \tau_C L_d + (1-\tau_C)L_C - L_S + (1-\rho_S)S_{d,s} \quad (Eq.9)$$

Sensible heat:

$$H = H_S + H_C = \rho c_p \frac{T_{AC} - T_A}{R_A} \quad (Eq.10)$$

$$H_S = \rho c_p \frac{T_S - T_{AC}}{R_S} \quad (Eq.11)$$

$$H_C = \rho c_p \frac{T_S - T_{AC}}{R_X} \quad (Eq.12)$$

Latent heat:

$$\lambda E = \lambda E_S + \lambda E_C \quad (Eq.13)$$

$$\lambda E_C = \alpha_C f_g \frac{S}{S+\gamma} RN_C \quad (Eq.14)$$

Soil conduction heat:

$$G = c_g \cos\left(\frac{2\pi\left[t_{g0} + 10800\right]}{t_g}\right) RN_S \quad (Eq.15)$$

Here, *RN* is net radiation, *H* is sensible heat, λE is latent heat, *G* is the soil heat conduction flux, *T* is temperature, *R* is a transport resistance, ρ is air density, c_p is the heat capacity of air at constant pressure, γ is the psychometric constant, and *S* is the slope of the saturation vapor pressure vs. temperature curve. The subscripts '*A*', '*AC*', and '*X*' signify properties of the air above and within the canopy, and within the leaf boundary layer, respectively, while '*S*' and '*C*' refer to fluxes and states associated with the soil and canopy components of the system. The soil heat conduction flux is computed as a diurnal function of the net radiation below the canopy, at the soil surface following Santanello and Friedl (2003). In Eq. 15, t_{g0} is the time (in seconds) from local noon. For a soil substrate, the parameters c_g and t_g are scaling factors that vary with soil moisture. In DisALEXI, the soil wetness regime is represented by a weighted function of the soil evaporative fraction:

$$c_g = w c_{gmax} + (1-w) c_{gmin}$$
$$t_g = w t_{gmax} + (1-w) t_{gmin}$$

where

$$w = \frac{1}{\left(1+\left[\frac{EF_S}{0.5}\right]^8\right)}$$
$$EF_S = \lambda E_S/(RN_S - G).$$

For a soil substrate, we use t_{gmax}=100000, t_{gmin}=74000, c_{gmax}=0.35, and c_{gmin}=0.31.

The TSEB has a built-in mechanism for detecting thermal signatures of vegetation stress. In the original TSEB form, a modified Priestley-Taylor relationship (PT; Priestley and Taylor 1972), applied to the divergence of net radiation within the canopy (RN_C), provides an initial estimate of canopy transpiration (λE_C) (Eq. 14), while the soil evaporation rate (λE_S) is computed as a residual to the system energy budget. If the vegetation is stressed and transpiring at significantly less than the potential rate, the PT equation will overestimate λE_C and the residual λE_S will become negative. Condensation onto the soil is unlikely during midday on clear days, and therefore $\lambda E_S <$ 0 is considered a signature of system stress. Under such circumstances, the PT coefficient, α, is iteratively reduced from its initial unstressed value (typically 1.26) until $\lambda E_S \sim 0$ (expected for dry conditions). Justification for this parameterization of λE_c is provided by Norman et al. (1995b) and Agam et al. (2010). Alternative forms for λE_c based on the Penman-Monteith equation (Colaizzi et al. 2014) or a light-use efficiency approach (Anderson et al. 2008) have also been developed – these tend to affect the partitioning between the λE_c and λE_s but not the combined evaporative flux.

The series resistance formalism described here allows both the soil and the vegetation to influence the microclimate within the canopy air space, as shown in Fig. 3. The resistances considered include R_A, the aerodynamic resistance for momentum between the canopy and the upper boundary of the model (including diabatic corrections); R_X, the bulk boundary layer resistance over all leaves in the canopy; and R_S, the resistance through the boundary layer immediately above the soil surface. Mathematical expressions for these resistance terms are given by Norman et al. (1995b).

In Eqs. 1-15, RN is the net radiation above the canopy, RN_C is the component absorbed by the canopy, and RN_S is the component penetrating to the soil surface. The longwave components of RN and RN_S are a function of the thermal radiation from the sky (L_d), the canopy (L_c) and the soil (L_s), and the coefficient of diffuse radiation transmission through the canopy (τ_c). The shortwave components depend on insolation values above the canopy (S_d) and above the soil surface ($S_{d,s}$), and the reflectivity of the soil-canopy system (A) and the soil surface itself (ρ_s). Based on the work of (Goudriaan 1977), Campbell and Norman (1998) provide analytical approximations for τ_c and A for sparse to deep canopies, depending on leaf absorptivity in the visible, near-infrared and thermal bands, ρ_s, and leaf area index (see App. B in Anderson et al. 2000 for further information).

4.2 Application of the TSEB using remotely sensed inputs

For applications of the TSEB, the equation set described in Sec. 4.1 is applied at every pixel in the modeling domain using T_{RAD}, LAI or f_c, and reflectance/albedo inputs from remote sensing products. Meteorological forcings of wind speed, atmospheric pressure, vapor pressure and insolation are obtained from local measurements or from a gridded reanalysis framework. Section 4.4 and 4.5 discuss methods for specifying the air temperature (T_A) boundary condition (Fig. 3),

while Section 4.6 describes sources of pixel-based inputs for ECOSTRESS ET mapping applications.

4.3 Upscaling from overpass time to daily total ET

ET (mass flux; kg s^{-1} m^{-2} or mm s^{-1}) is computed from latent heat flux λE (energy flux; Wm^{-2} or $Jm^{-2}s^{-1}$) by dividing by the latent heat of vaporization required to evaporate a unit of water (λ; J kg^{-1} or J mm^{-1}). TSEB ET values are upscaled from instantaneous values (λE_{inst}) retrieved at the satellite overpass time to daily total values (ETd) using the ratio of instantaneous to daily insolation:

$$ETd = f_{SUN} * Rs_{24}/\lambda$$

$$f_{SUN} = \lambda E_{inst}/Rs_{inst} \qquad \text{(Eq. 2)}$$

where f_{SUN} is the ratio of instantaneous latent heat to instantaneous insolation image at overpass time, and Rs_{24} is the time-integrated daily insolation rate. While evaporative fraction $\lambda E/(Rn-G)$ is often used to accomplish upscaling to daily total ET, studies have demonstrated that f_{sun} provides comparable results and is less susceptible to errors in retrieval of Rn and G (Van Niel et al. 2012; 2011; Cammalleri et al. 2014b).

Dependence of satellite overpass time on errors in daily upscaling will be further evaluated using diurnally varying ECOSTRESS retrievals from the ISS.

4.4 Regional applications of TSEB (ALEXI)

One of the biggest challenges in a regional implementation of the TSEB is to adequately define the air temperature boundary condition, T_A, over the modeling domain (Fig. 3). While lower boundary conditions are supplied by thermal remote-sensing data, the TSEB requires specification of temperature above the canopy and is particularly sensitive to biases in this input with respect to the TIR reference (Zhan et al. 1996; Anderson et al. 1997; Kustas and Norman 1997). Small biases in T_A with respect to T_{RAD} can significantly corrupt model estimates of H, and therefore λE by residual – by up to ~100 Wm^{-2} per ^oC depending on surface and meteorological conditions (Norman et al. 1995a). Significant biases in the measured surface-to-air temperature gradient should be expected due to local land-atmosphere feedback not captured in the gridded T_A field (typically generated either through mesoscale analysis or direct interpolation of synoptic weather station data).

For regional-scale applications, the TSEB has been coupled in time-differencing mode with an atmospheric boundary layer (ABL) model to internally simulate land-atmosphere feedback on near-surface air temperature (T_A), and to minimize impacts of errors in LST retrieval. In the ALEXI model, the TSEB is applied at two times (t_1 and t_2) during the morning ABL growth phase (~1 hr after sunrise and before local noon) using radiometric temperature data obtained from a geostationary platform, typically at spatial resolutions of 3-10 km. ALEXI assumes a linear increase in H between t_1 and t_2, and thus cloud-free conditions are required in the interim. Energy closure over this interval is provided by a simple slab model of ABL development (McNaughton and Spriggs 1986), which relates the rise in air temperature in the mixed layer to the time-integrated influx of sensible heat from the land surface. As a result of this configuration, ALEXI

uses only time-differential temperature signals, thereby minimizing flux errors due to absolute sensor calibration, as well as atmospheric and emissivity corrections (Anderson et al. 1997; Kustas et al. 2001). The primary radiometric signal is the morning surface temperature rise, while the ABL model component uses only the general slope (lapse rate) of the atmospheric temperature profile (Anderson et al. 1997), which is more reliably analyzed from synoptic radiosonde data than is the absolute temperature reference.

ALEXI has been transitioned to operational production by the National Oceanic and Atmospheric Administration (NOAA) Office of Satellite and Product Operations (OSPO) as the core model of their GOES Evapotranspiration and Drought Product (GET-D) system. ALEXI ET retrievals at 4-8km resolution support NOAA land-surface modeling verification and drought monitoring over the North American continent. Details on the GET-D ALEXI implementation can be found in the NOAA GET-D ALEXI ATBD.

4.5 DisALEXI-JPL disaggregation scheme

For finer resolution assessments (smaller scales than can be provided by geostationary imagery), an ALEXI flux disaggregation scheme (DisALEXI) has been developed, with the combined system designed to generate consistent flux maps over a range in spatial scales – from continental coverage at 3-10 km resolution, to local area coverage at 1-1000 m resolution (Norman et al. 2003; Anderson et al. 2004b). The air temperature field, T_A, diagnosed by ALEXI at time t_2 serves as an initial upper boundary condition at a nominal blending height for a gridded implementation of the TSEB, which uses higher resolution LST and LAI data from polar orbiting systems like Landsat, MODIS, VIIRS, or in this case from ECOSTRESS (Fig. 3). This air temperature boundary is iteratively modified on the scale of an ALEXI pixel such that the average daily ET flux from DisALEXI-JPL matches the coarser scale ALEXI flux (Anderson et al. 2012). This ensures consistency between ALEXI and DisALEXI flux distributions at the ALEXI pixel scale.

4.6 Inputs for ECOSTRESS applications

Input datasets used for ECOSTRESS ET retrievals using DisALEXI-JPL are listed in Table 1. Because ECOSTRESS does not include the shortwave bands required to specify albedo and vegetation cover inputs required by DisALEXI-JPL, these inputs must be interpolated to the ECOSTRESS overpass date from other sources (e.g., Landsat).

Table 1. Primary inputs used by DisALEXI-JPL for ECOSTRESS applications.

Data	Purpose	Source	Spatial Resolution
LST	T_{RAD}, Rn	ECOSTRESS	~70 m
Surface reflectance	Albedo	Landsat	30 m
LAI	T_{RAD} partitioning	MODIS/Landsat	30 m
Insolation	Rn	CFSR	0.25 °
Wind speed	Aerodynamic resistances	CFSR	0.25 °
Air temperature	Preliminary boundary cond.	CFSR	0.25 °
Atm. pressure	Surface coefficients	CFSR	0.25 °
Vapor pressure	Surface coefficients	CFSR	0.25 °

Landcover type	Canopy characteristics	NLCD	30 m

4.6.1 T_{RAD}

Surface radiometric temperature, T_{RAD}, used in Eq. 2 is obtained from standard ECOSTRESS LST products at 70-m resolution. DisALEXI-JPL is produced at native ECOSTRESS swath resolution, and it is an extension of the DisALEXI-USDA product that is made available over select sites at 30 m spatial resolution.

4.6.2 Meteorological data

Hourly insolation, temperature, wind and pressure fields were obtained from the Climate Forecast System Reanalysis dataset (Saha et al. 2010), also used in the ALEXI GET-D production system. These fields are resampled to the 30-m DisALEXI-JPL grid at hourly timesteps for ingestion into DisALEXI-JPL. Resampling from 0.25° to 30-m is accomplished through nearest neighbor assignment, followed by Gaussian smoothing to reduce coarse resolution artifacts in the ET retrievals at the CFSR pixel scale.

4.6.3 Landcover classification

Satellite-derived fractional cover estimates have been used in conjunction with a gridded land-surface classification to assign relevant surface parameters such as roughness length and radiometric properties. For ECOSTRESS ET products, the processing employs the 2011 National Land Cover Dataset (NLCD) at 30-m resolution, which contains 29 vegetation classes (Homer et al. 2015). Pixel level values of leaf size (used in determining canopy boundary layer resistance, R_x) and leaf absorptivity in the visible, near-infrared, and thermal wavebands (α_{vis}, α_{NIR}, and α_{TIR}; used in net radiation partitioning) are assigned based on a class-based look-up table (Table 2). See Anderson et al. (2007b) for details on how these parameters are used in computing TSEB variables.

Table 2. Landcover classification system used in DisALEXI-JPL over CONUS, along with parameters that vary according to landcover class including the seasonal maximum and minimum canopy heights (h_{max} and h_{min}), leaf absorptivity (α) in the visible, NIR, and TIR bands, and nominal leaf size (s). The DisALEXI-JPL classification system is based on the NLCD datasets.

Class	Description	h_{min} (m)	h_{max} (m)	α_{vis}	α_{NIR}	α_{TIR}	s (m)
1	Open Water	0.1	0.6	0.82	0.28	0.95	0.02
2	Perennial Ice/Snow	0.1	0.6	0.82	0.28	0.95	0.02
3	Developed Open Space	0.1	0.6	0.84	0.37	0.95	0.02
4	Developed Low Intensity	0.1	0.6	0.84	0.37	0.95	0.02
5	Developed Medium Intensity	1	1	0.84	0.37	0.95	0.02
6	Developed High Intensity	6	6	0.84	0.37	0.95	0.02
7	Barren Land	0.1	0.2	0.82	0.57	0.95	0.02
8	Unconsolidated Shore	0.1	0.2	0.82	0.57	0.95	0.02
9	Deciduous Forest	10	10	0.86	0.37	0.95	0.1
10	Evergreen Forest	15	15	0.89	0.6	0.95	0.05

11	Mixed Forest	12	12	0.87	0.48	0.95	0.08
12	Dwarf Scrub	0.2	0.2	0.83	0.35	0.95	0.02
13	Shrub Scrub	1	1	0.83	0.35	0.95	0.02
14	Grasslands Herbaceous	0.1	0.6	0.82	0.28	0.95	0.02
15	Sedge Herbaceous	0.1	0.6	0.82	0.28	0.95	0.02
16	Lichens	0.1	0.1	0.82	0.28	0.95	0.02
17	Moss	0.1	0.1	0.82	0.28	0.95	0.02
18	Pasture Hay	0.1	0.6	0.82	0.28	0.95	0.02
19	Cultivated Crops	0.1	0.6	0.83	0.35	0.95	0.05
20	Woody Wetlands	5	5	0.85	0.36	0.95	0.05
21	Palustrine Forested Wetland	1	2.5	0.85	0.36	0.95	0.05
22	Palustrine Scrub Shrub Wetland	1	2.5	0.85	0.36	0.95	0.05
23	Estuarine Forested Wetland	1	2.5	0.85	0.36	0.95	0.05
24	Estuarine Scrub Shrub Wetland	1	2.5	0.85	0.36	0.95	0.05
25	Emergent Herbaceous Wetland	1	2.5	0.85	0.36	0.95	0.05
26	Palustrine Emergent Wetland	1	2.5	0.85	0.36	0.95	0.05
27	Estuarine Emergent Wetland	1	2.5	0.85	0.36	0.95	0.05
28	Palustrine Aquatic Bed	1	2.5	0.85	0.36	0.95	0.05
29	Estuarine Aquatic Bed	1	2.5	0.85	0.36	0.95	0.05

4.6.4 LAI and cover fraction

The ECOSTRESS resolution LAI maps used for ECOSTRESS ET mapping are generated using a linear interpolation between MODIS LAI and Landsat NDVI, resampled to MODIS resolution. The resulting scaling factor is used to estimate ECOSTRESS-resolution LAI when applied to Landsat. This method may not be accurate at high LAI, and will likely be improved in later versions. Cover fraction at nadir view, *f(0)*, is computed from LAI using Eq. 3.

4.6.5 Roughness parameters

To simulate phenological changes in surface roughness properties, the model input canopy height has been tied to both class and vegetation cover fraction. Within each class, canopy height is scaled linearly with *f(0)* between a seasonal minimum and maximum value (see Table 2):

$$h_{c,i} = h_{c\min,i} + f(0)\left[h_{c\max,i} - h_{c\min,i}\right] \quad (18)$$

and then the momentum roughness ($z_{o,i}$) and displacement height (d_i) parameters are computed for each class as cover-dependent fractions of the canopy height (Massman 1997). Aerodynamic, soil and canopy resistance factors are specified individually for each grid cell within the modeling domain based on the roughness and meteorological characteristics assigned to that cell.

4.6.6 Soil and leaf optical properties

Broadband visible and near-infrared albedo for each pixel are extracted from the six Landsat reflectance bands in the SR CDR according to Liang et al. (2000). Given vegetation class-dependent specifications of leaf absorptivity parameters (Table 2), soil reflectance in each cell is

iteratively adjusted from a nominal value until the computed pixel-level composite albedo matches the measured values in these two broad bands.

5 Data Processing

The DisALEXI-JPL processing stream is schematized in Fig. 4.

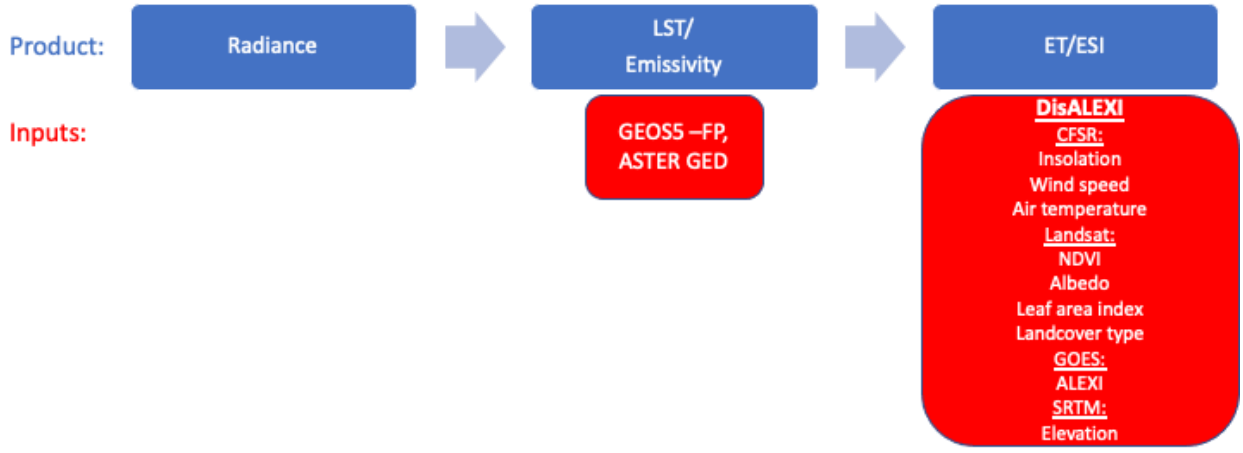

Figure 4. Conceptual diagram describing computation of L3 (ECO3ETALEXI) evapotranspiration along with required inputs.

The input ingestion component of the system retrieves all required input datasets and resamples them to native ECOSTRESS resolution. Landsat surface reflectance (SR), Climate Data Record (CDR) products and MODIS LAI product tiles over the study areas are collected using an automated downloader/preprocessor tool designed by JPL. ALEXI and CFSR datasets are obtained from NASA Marshall Space Flight Center via FTP. To facilitate near-real-time processing, the Landsat and MODIS acquisitions acquired closest historically to the ECOSTRESS acquisition are used. The DisALEXI-JPL code is fully implemented in Python, and the data is delivered to the Land Processes Distributed Active Archive Center (LP DAAC) for dissemination.

6 Model Evaluation

The ECOSTRESS L3(ALEXI_ET) products were evaluated at points throughout the contiguous United States (CONUS) sampled by existing eddy covariance (EC) tower ET measurement sites. Selected target regions focus on sites within the AmeriFlux and NEON networks.

Ancillary meteorological data, net radiation (four components where available), soil heat, and sensible and latent heat flux data collected at these tower sites were aggregated to daily timesteps. EC data are subject to energy budget closure errors, such that often $RN - G > \lambda E + H$ (Twine et al. 2000; Wilson et al. 2002). To improve consistency with the model, which enforces closure through Eq. 1, the fluxes were used as measured and with a correction assigning the residual closure error to the latent heat flux (Prueger et al. 2005). Uncertainties in observed fluxes are often reflected in these closure errors, with the true value likely bracketed between closed and unclosed flux measurements (Alfieri et al. 2011).

For comparison with tower flux measurements, instantaneous and daily surface energy balance component retrievals, as well as daily ET, were extracted from the DisALEXI-JPL ET timeseries.

Standard statistical metrics of model performance were computed, including bias and root mean squared error (RMSE).

This product was evaluated at 17 CONUS flux sites over a variety of landcover types, yielding accuracies with $R^2 = 0.8$ and RMSE = 0.81 mm/day (Figure 1), which is comparable to previous DisALEXI validation studies (Cawse-Nicholson et al., in review). This validation also shows the impact of quality flags, as pixels with high view zenith angles or high aerosol optical depth showed greater deviation from field measurements.

7 Uncertainty

Understanding the uncertainty associated with DisALEXI-JPL ET is vital for science predictions and analysis and for water resource management decision making. In Cawse-Nicholson et al., (2020), the uncertainty is statistically quantified. DisALEXI depends on ECOSTRESS LST as well ancillary inputs for landcover, elevation, vegetation parameters, and meteorological inputs. Since each of these inputs has an associated, and potentially unknown, uncertainty, in this study a Monte Carlo simulation based on a spatial statistical model was used to determine the algorithms sensitivity to each of its inputs, and to quantify the probability distribution of algorithm outputs. Analysis showed that algorithm is most sensitive to LST (the input derived from ECOSTRESS). Significantly, the output uncertainty distribution is non-Gaussian, due to the non-linear nature of the algorithm. Here, uncertainty was represented using five quantiles of the output distribution. The distribution was consistent across five different datasets (mean offset is 0.01 mm/day, and 95% of the data is contained within 0.3 mm/day). An additional two datasets with low ET, showed higher uncertainty (95% of the data is within 1 mm/day), and a positive bias (i.e. ET was overestimated by an average of 0.12 mm/day when ET was low).

Since LST is the only input provided with an associated uncertainty estimate, we derived a linear regression between LST uncertainty and ET uncertainty in this experiment, and that relationship is propagated to all DisALEXI-JPL ET products.

8 Metadata

- unit of measurement: Watts per square meter (mm d-1)
- range of measurement: 0 to 10 mm d^{-1}
- projection: ECOSTRESS
- spatial resolution: ECOSTRESS (70 m at nadir)
- temporal resolution: dynamically varying with precessing ISS overpass; represents daily value on day of overpass, local time
- spatial extent: CONUS
- start date time: near real-time
- end data time: near real-time
- number of bands: not applicable
- data type: float
- min value: 0
- max value: X
- no data value: 9999
- bad data values: 9999
- flags: quality level 1-4 (best to worst)

9 Acknowledgements

We thank Martha Anderson, Munish Sikka, Erin Wong, Gregory Halverson, Chris Hain, Feng Gao, Bill Kustas, John Norman, Carmelo Cammalleri, Peijuan Wang, Kate Semmens, Yun Yang, Wayne Dulaney, Liang Sun, and Yang Yang for contributions to the algorithm development described in this ATBD.

10 References

Agam, N., Kustas, W.P., Anderson, M.C., Norman, J.M., Colaizzi, P.D., & Prueger, J.H. (2010). Application of the Priestley-Taylor approach in a two-source surface energy balance model. *J. Hydrometeorology, 11*, 185-198

Alfieri, J.G., Kustas, W.P., Prueger, J.H., Hipps, L.E., Chavez, J.L., French, A.N., & Evett, S.R. (2011). Intercomparison of nine micrometeorological stations during the BEAREX08 field campaign. *J Atmos Oceanic Tech.*

Anderson, M.C., Norman, J.M., Diak, G.R., Kustas, W.P., & Mecikalski, J.R. (1997). A two-source time-integrated model for estimating surface fluxes using thermal infrared remote sensing. *Remote Sens. Environ., 60*, 195-216

Anderson, M.C., Norman, J.M., Meyers, T.P., & Diak, G.R. (2000). An analytical model for estimating canopy transpiration and carbon assimilation fluxes based on canopy light-use efficiency. *Agric. For. Meteorol., 101*, 265-289

Anderson, M.C., Kustas, W.P., & Norman, J.M. (2003). Upscaling and downscaling - a regional view of the soil-plant-atmosphere continuum. *Agron. J., 95*, 1408-1423

Anderson, M.C., Neale, C.M.U., Li, F., Norman, J.M., Kustas, W.P., Jayanthi, H., & Chavez, J. (2004a). Upscaling ground observations of vegetation water content, canopy height, and leaf area index during SMEX02 using aircraft and Landsat imagery. *Remote Sens. Environ., 92*, 447-464

Anderson, M.C., Norman, J.M., Mecikalski, J.R., Torn, R.D., Kustas, W.P., & Basara, J.B. (2004b). A multi-scale remote sensing model for disaggregating regional fluxes to micrometeorological scales. *J. Hydrometeor., 5*, 343-363

Anderson, M.C., Norman, J.M., Kustas, W.P., Li, F., Prueger, J.H., & Mecikalski, J.M. (2005). Effects of vegetation clumping on two-source model estimates of surface energy fluxes from an agricultural landscape during SMACEX. *J. Hydrometeorol., 6*, 892-909

Anderson, M.C., Kustas, W.P., & Norman, J.M. (2007a). Upscaling flux observations from local to continental scales using thermal remote sensing. *Agron. J., 99*, 240-254

Anderson, M.C., Norman, J.M., Mecikalski, J.R., Otkin, J.A., & Kustas, W.P. (2007b). A climatological study of evapotranspiration and moisture stress across the continental U.S. based on thermal remote sensing: I. Model formulation. *J. Geophys. Res., 112, D10117, doi:10.1029/2006JD007506*

Anderson, M.C., Norman, J.M., Kustas, W.P., Houborg, R., Starks, P.J., & Agam, N. (2008). A thermal-based remote sensing technique for routine mapping of land-surface carbon, water and energy fluxes from field to regional scales. *Remote Sens. Environ., 112*, 4227-4241

Anderson, M. C., Kustas, W. P., Norman, J. M., Hain, C. R., Mecikalski, J. R., Schultz, L., Gonzalez-Dugo, M. P., Cammalleri, C., D'Urso, G. , Pimstein, A. and Gao, F. Mapping daily evapotranspiration at field to continental scales using geostationary and polar orbiting satellite imagery. *Hydrol. Earth Syst. Sci.*, 15, 223–239, 2011.

Anderson, M.C., Kustas, W.P., Alfieri, J.G., Hain, C.R., Prueger, J.H., Evett, S.R., Colaizzi, P.D., Howell, T.A., & Chavez, J.L. (2012). Mapping daily evapotranspiration at Landsat spatial scales during the BEAREX'08 field campaign. *Adv. Water Resour., 50*, 162-177

Cammalleri, C., Anderson, M.C., Ciraolo, G., D'Urso, G., Kustas, W.P., La Loggia, G., & Minacapilli, M. (2012). Applications of a remote sensing-based two-source energy balance

algorithm for mapping surface fluxes without in situ air temperature observations. *Remote Sensing of Environment, 124*, 502-515

Cammalleri, C., Anderson, M.C., Gao, F., Hain, C.R., & Kustas, W.P. (2013). A data fusion approach for mapping daily evapotranspiration at field scale. *Water Resources Res., 49*, 1-15, doi:10.1002/wrcr.20349

Cammalleri, C., Anderson, M.C., Gao, F.H., C.R., & Kustas, W.P. (2014a). Mapping daily evapotranspiration at field scales over rainfed and irrigated agricultural areas using remote sensing data fusion. *Agric. For. Meteorol., 186*, 1-11

Cammalleri, C., Anderson, M.C., & Kustas, W.P. (2014b). Upscaling of evapotranspiration fluxes from instantaneous to daytime scales for thermal remote sensing applications. *Hydrol. Earth Syst. Sci., 18*, 1885-1894

Cawse-Nicholson, K., Anderson, M., Yang, Y., Yang, Y., Hook, S., Fisher, J.B., Halverson, G., Hulley, G., Hain, C., Brunsell, N.A., Desai, A.R., Novick, K.A. (2021 in review) Evaluation of a CONUS-wide ECOSTRESS DisALEXI evapotranspiration product. IEEE Journal of Selected Topics in Applied Remote Sensing.

Cawse-Nicholson, K. et al. (2020). Sensitivity and uncertainty quantification for the ECOSTRESS evapotranspiration algorithm - DisALEXI. International Journal of Applied Earth Observation and Geoinformation, vol. 89, p. 10208. https://doi.org/10.1016/j.jag.2020.102088.

Colaizzi, P.D., Agam, N., Tolk, J.A., Evett, S.R., Howell, T.A., Gowda, P.H., O'Shaughnessy, S.A., Kustas, W.P., & Anderson, M.C. (2014). Two-source energy balance model to calculate E, T, and ET: Comparison of priestley-taylor and penman-monteith formulations and two time scaling methods. *Trans ASABE, 57*, 479-498

Fisher, J.B., Hook, R., Allen, R.G., Anderson, M.C., French, A.N., Hain, C.R., Hulley, G., & Wood, E.F. (2014). The ECOsystem Spaceborne Thermal Radiometer Experiment on Space Station (ECOSTRESS): science motivation. In, *American Geophysical Union Fall Meeting*. San Francisco, CA

J. B. Fisher, B. Lee, A. J. Purdy, G. H. Halverson, M. B. Dohlen, K. Cawse-Nicholson, et al., "ECOSTRESS: Nasa's next generation mission to measure evapotranspiration from the International Space Station," *Water Resources Research*, vol. 56, no. 4, p. e2019WR026058, 2020.

Gao, F., Anderson, M.C., Kustas, W.P., & Wang, Y. (2012a). A simple method for retrieving Leaf Area Index from Landsat using MODIS LAI products as reference. *J. Appl. Remote Sensing, 6*, DOI: 10.1117/.JRS.1116.063554

Gao, F., Kustas, W.P., & Anderson, M.C. (2012b). A data mining approach for sharpening thermal satellite imagery over land. *Remote Sensing, 4*, 3287-3319

Goudriaan, J. (1977). *Crop micrometeorology: a simulation study*. Wageningen: Simulation Monographs

Homer, C., Dewitz, J., Yang, L., Jin, S., Danielson, P., Xian, G., Coulston, J., Herold, N., Wickham, J., & Megown, K. (2015). Completion of the 2011 National Land Cover Databawse for the Conterminous United States - Representing a decade of land cover change information. *Photogramm. Eng. and Remote Sensing, 81*, 345-354

Hsieh, C.I., Katul, G., & Chi, T.W. (2000). An approximate analytical model for footprint estimation of scalar fluxes in thermally stratified atmospheric flows. *Adv. Water Resour., 23*, 765-772

Hulley, G. (2018) Level-2 Land Surface Temperature and Emissivity Algorithm Theoretical Basis Document. https://ecostress.jpl.nasa.gov/documents/atbds-summary-table

Kalma, J.D., McVicar, T.R., & McCabe, M.F. (2008). Estimating land surface evaporation: A review of methods using remotely sensing surface temperature data. *Survey Geophys.,* DOI 10.1007/s10712-10008-19037-z

Kustas, W.P., & Norman, J.M. (1997). A two-source approach for estimating turbulent fluxes using multiple angle thermal infrared obserations. *Water Resources Research, 33,* 1495-1508

Kustas, W.P., & Norman, J.M. (1999). Evaluation of soil and vegetation heat flux predictions using a simple two-source model with radiometric temperatures for partial canopy cover. *Agric. For. Meteorol., 94,* 13-29

Kustas, W.P., & Norman, J.M. (2000). A two-source energy balance approach using directional radiometric temperature observations for sparse canopy covered surfaces. *Agronomy J., 92,* 847-854

Kustas, W.P., Diak, G.R., & Norman, J.M. (2001). Time difference methods for monitoring regional scale heat fluxes with remote sensing. *Land Surface Hydrology, Meteorology, and Climate: Observations and Modeling, 3,* 15-29

Kustas, W.P., & Anderson, M.C. (2009). Advances in thermal infrared remote sensing for land surface modeling. *Agric. For. Meteorol., 149,* 2071-2081

Li, F., Kustas, W.P., Anderson, M.C., Prueger, J.H., & Scott, R.L. (2008). Effect of remote sensing spatial resolution on interpreting tower-based flux observations. *Remote Sens. Environ., 112,* 337-349

Liang, S. (2000). Narrowband to broadband conversions of land surface albedo I Algorithms. *Remote Sens. Environ., 76,* 213-238

Massman, W. (1997). An analytical one-dimensional model of momentum transfer by vegetation of arbitrary structure. *Bound.-Layer Meteor., 83,* 407-421

McNaughton, K.G., & Spriggs, T.W. (1986). A mixed-layer model for regional evaporation. *Boundary-Layer Meteorol., 74,* 262-288

Norman, J.M., Divakarla, M., & Goel, N.S. (1995a). Algorithms for extracting information from remote thermal-IR observations of the earth's surface. *Remote Sens. Environ., 51,* 157-168

Norman, J.M., Kustas, W.P., & Humes, K.S. (1995b). A two-source approach for estimating soil and vegetation energy fluxes from observations of directional radiometric surface temperature. *Agric. For. Meteorol., 77,* 263-293

Norman, J.M., Anderson, M.C., Kustas, W.P., French, A.N., Mecikalski, J.R., Torn, R.D., Diak, G.R., Schmugge, T.J., & Tanner, B.C.W. (2003). Remote sensing of surface energy fluxes at 10^1-m pixel resolutions. *Water Resour. Res., 39,* DOI:10.1029/2002WR001775

Priestley, C.H.B., & Taylor, R.J. (1972). On the assessment of surface heat flux and evaporation using large-scale parameters. *Mon. Weather Rev., 100,* 81-92

Prueger, J.H., Hatfield, J.L., Kustas, W.P., Hipps, L.E., MacPherson, J.I., & Parkin, T.B. (2005). Tower and aircraft eddy covariance measurements of water vapor, energy and carbon dioxide fluxes during SMACEX. *J. Hydrometeor., 6,* 954-960

Saha, S., Moorthi, S., Pan, H.-L., Wu, X., & Coauthors (2010). The NCEP Climate Forecast System Reanalysis. *Bull. Amer. Meteorol. Soc., 91,* 1015-1057

Santanello, J.A., & Friedl, M.A. (2003). Diurnal variation in soil heat flux and net radiation. *J. Appl. Meteorol., 42*, 851-862

Semmens, K.A., Anderson, M.C., Kustas, W.P., Gao, F., Alfieri, J.G., McKee, L., Prueger, J.H., Hain, C.R., Cammalleri, C., Yang, Y., Xia, T., Vélez, M., Sanchez, L., & Alsina, M. (2015). Monitoring daily evapotranspiration over two California vineyards using Landsat 8 in a multi-sensor data fusion approach. *Remote Sens. Environ.*, doi:10.1016/j.rse.2015.1010.1025

Sun, L., Anderson, M.C., Gao, F., Hain, C.R., Alfieri, J.G., Sharifi, A., McCarty, G., Yang, Y., & Yang, Y. (2017). Investigating water use over the Choptank River Watershed using a multi-satellite data fusion approach. *Water Resources Res., 53*, 5298-5319

Twine, T.E., Kustas, W.P., Norman, J.M., Cook, D.R., Houser, P.R., Meyers, T.P., Prueger, J.H., Starks, P.J., & Wesely, M.L. (2000). Correcting eddy-covariance flux underestimates over a grassland. *Agric. For. Meteorol., 103*, 279-300

Van Niel, T.G., McVicar, T.R., Roderick, M.L., Van Dijk, A.I.J.M., Renzullo, L.J., & Van Gorsel, E. (2011). Correcting for systematic error in satellite-derived latent heat flux due to assumptions in temporal scaling : Assessment from flux tower observations. *J. Hydrol., 409*, 140-148

Van Niel, T.G., McVicar, T.R., Roderick, M.L., Van Dijk, A.I.J.M., Beringer, J., Hutley, L.B., & Van Gorsel, E. (2012). Upscaling latent heat flux for thermal remote sensing studies : Comparison of alternative approaches and correction of bias. *J. Hydrol., 468–469*, 35–46

Wilson, K., Goldstein, A., Falge, E., Aubinet, M., Baldocchi, D., Berbigier, P., Bernhofer, C., Ceulemans, R., Dolman, H., Field, C., Grelle, A., Ibrom, A., Law, B.E., Kowalski, A., Meyers, T., Moncrieff, J., Monson, R., Oechel, W., Tenhunen, J., Valentini, R., & Verma, S. (2002). Energy balance closure at FLUXNET sites. *Agric. For. Meteorol., 113*, 223-243

Yang, Y., Anderson, M.C., Gao, F., Hain, C., Kustas, W.P., Meyers, T., Crow, W., Finocchiaro, R.G., Otkin, J.A., Sun, L., & Yang, Y. (2017a). Impact of tile drainage on evapotranspiration (ET) in South Dakota, USA based on high spatiotemporal resolution ET timeseries from a multi-satellite data fusion system. *J. Selected Topics in Applied Earth Obs. and Remote Sensing, 10*, 2550 - 2564

Yang, Y., Anderson, M.C., Gao, F., Hain, C.R., Semmens, K.A., Kustas, W.P., Normeets, A., Wynne, R.H., Thomas, V.A., & Sun, G. (2017b). Daily Landsat-scale evapotranspiration estimation over a managed pine plantation in North Carolina, USA using multi-satellite data fusion. *Hydrol. Earth Syst. Sci., 21*, 1017-1037

Zhan, X., Kustas, W.P., & Humes, K.S. (1996). An intercomparison study on models of sensible heat flux over partial canopy surfaces with remotely sensed surface temperatures. *Remote Sens. Environ., 58*, 242-256